Project Prometheus at UCLA

Team 108 Project Technical Report for the 2018 IREC

Caleb Lessard-Clouston[1]
Mechanical and Aerospace Engineering Department, Los Angeles, California, 90024

Anneliese Peterson[2]
Mechanical and Aerospace Engineering Department, Los Angeles, California, 90024

Alexander Lima[3]
Mechanical and Aerospace Engineering Department, Los Angeles, California, 90024

Anthony Smolyanov[4]
Mechanical and Aerospace Engineering Department, Los Angeles, California, 90024

Sienna Stinson[5]
Mechanical and Aerospace Engineering Department, Los Angeles, California, 90024

Sipora Shaolian[6]
Mechanical and Aerospace Engineering Department, Los Angeles, California, 90024

Nora Stacy[7]
Mechanical and Aerospace Engineering Department, Los Angeles, California, 90024

Jason Feldkamp[8]
Mechanical and Aerospace Engineering Department, Los Angeles, California, 90024

Olivia Wesel[9]
Mechanical and Aerospace Engineering Department, Los Angeles, California, 90024

Hayley Martinez[10]
Computer Science and Engineering Department, Los Angeles, California, 90024

Connor Matro[11]
Mechanical and Aerospace Engineering Department, Los Angeles, California, 90024

[1] Mechanical and Aerospace Engineering Department, Los Angeles, California, 90024.
[2] Mechanical and Aerospace Engineering Department, Los Angeles, California, 90024.
[3] Mechanical and Aerospace Engineering Department, Los Angeles, California, 90024.
[4] Mechanical and Aerospace Engineering Department, Los Angeles, California, 90024.
[5] Mechanical and Aerospace Engineering Department, Los Angeles, California, 90024.
[6] Mechanical and Aerospace Engineering Department, Los Angeles, California, 90024.
[7] Mechanical and Aerospace Engineering Department, Los Angeles, California, 90024.
[8] Mechanical and Aerospace Engineering Department, Los Angeles, California, 90024.
[9] Mechanical and Aerospace Engineering Department, Los Angeles, California, 90024.
[10] Computer Science and Engineering Department, Los Angeles, California, 90024.
[11] Mechanical and Aerospace Engineering Department, Los Angeles, California, 90024.

Christopher Vincent[12]
Mechanical and Aerospace Engineering Department, Los Angeles, California, 90024

Dr. Daniel Pineda[13]
Mechanical and Aerospace Engineering Department, Los Angeles, California, 90024

Dr. Mitchell Spearrin[14]
Mechanical and Aerospace Engineering Department, Los Angeles, California, 90024

and

Dr. Richard Wirz[15]
Mechanical and Aerospace Engineering Department, Los Angeles, California, 90024

Project Prometheus of Rocket Project at UCLA will be competing in the 10,000 ft AGL Apogee with Student Researched and Designed/Developed (SRAD) Hybrid or Liquid Rocket Propulsion System category with a completely student-manufactured hybrid motor. Team members redesigned and manufactured the Contrail M1575 to maximize performance. The rocket, *Hyperion*, will carry a CubeSat payload to collect in-flight data about Hyperion's trajectory and external environment to assist in future designs. Because Project Prometheus is largely comprised of underclassmen and new members, our three main objectives are innovation, achievement, and most importantly, education.

Nomenclature

$v_{off\text{-}rail}$	=	Off the rail speed
v_{wind}	=	Velocity of the wind
AOA	=	Angle of attack
Xc_p	=	Position of the center of pressure
Xcg	=	Position of the center of gravity
CC	=	Combustion chamber

PROJECT Prometheus is a new team under the rapidly expanding Rocket Project at UCLA. Of our 40 members, 64% are first year students at UCLA, 25% are second years, and nearly all members are new to Rocket Project. Our team prides itself on being open to all majors and experience levels to allow students to gain practical hands-on engineering experience. Our team is comprised of three subteams: Airframe, Propulsion, and Avionics. Each subteam has a chief engineer and team manager to organize meetings, oversee communication, and make final design decisions. Airframe designed and manufactured the aeroshell, fins, nosecone, and motor retainment system. Propulsion optimized and remanufactured the Contrail M-1575 hybrid motor. Avionics designed *Hyperion's* recovery system and built our CubeSat payload. The three subteams worked together to build an integrated system with cohesive parts with the support of the UCLA Mechanical and Aerospace Engineering department and alumni advisors.

[12] Mechanical and Aerospace Engineering Department, Los Angeles, California, 90024.
[13] Mechanical and Aerospace Engineering Department, Los Angeles, California, 90024.
[14] Mechanical and Aerospace Engineering Department, Los Angeles, California, 90024.
[15] Mechanical and Aerospace Engineering Department, Los Angeles, California, 90024.

I. System Architecture Overview

Figure II.1. Rendering of *Hyperion* as it will be flown at the Spaceport America Cup

A. Propulsion Subsystems

Figure II.2. Cutaway rendering of motor

The propulsion subsystem consists of a single student researched and designed hybrid motor. This motor is an optimized and remanufactured commercial motor (Contrail M-1575). Liquid nitrous oxide is used as the oxidizer in this system, while a paraffin wax/HTPB mixture is used as the solid fuel grain. The motor consists of an oxidizer tank and combustion chamber connected to each other by a coupler containing the injector plate. The motor utilizes a blow-down feed system relying on the self-pressurizing nature of nitrous oxide at operating temperature.

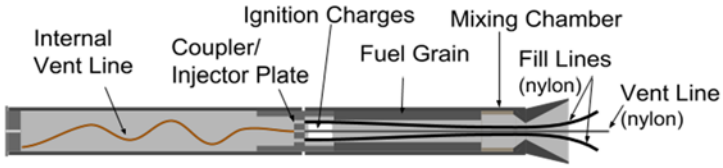

Figure II.3. Motor component diagram

The motor utilizes a novel fill system that is composed of push-to-connect fittings which serve as injectors and as fill inlets. To fill, nylon tubes are connected to four radial push-to-connects and nitrous flows into the oxidizer tank due to the pressure difference between the supply bottle and oxidizer tank. This pressure drop is maintained via a controlled vent. The vent line is connected to a push-to-connect in the center of the injector face. On the opposite side of the injector plate, inside the oxidizer tank, is a metal vent tube that runs to the top of the tank and ensures gaseous nitrous is vented rather than liquid until fill is complete. The vent and fill lines run through the fuel grain and out the nozzle during vent.

Ignition charges composed of a potassium nitrate-sugar mixture and wrapped in nichrome wire are placed on each of the fill lines. When the charges ignite, they serve a dual purpose of burning through the fill lines, disconnecting the rocket from ground plumbing and beginning oxidizer flow, and igniting the fuel and oxidizer mixture beginning thrust-producing combustion. The excess nylon tubes are then ejected out of the combustion chamber through the nozzle.

On the combustion chamber side of the injector plate, there is an approximately one inch-long cavity that serves as a preheating chamber for the nitrous oxide to reduce combustion instability. The fuel grain then extends for 18 inches and is followed by a 1.75 inch mixing chamber that ensures more complete combustion, thus increasing

efficiency. The nozzle is a commercial nozzle composed of a graphite converging section and conical aluminum diverging section.

Table II.1 highlights the performance and mass characteristics of the SRAD motor compared to the commercial system we began our optimizations with.

	COTS	SRAD	Change		COTS	SRAD	Change
Avg Thrust (lbf)	350.	395	+12.9%	Dry Mass (lbm)	21.16	16.73	-21%
Max Thrust (lbf)	666	723	+8.6%	Wet Mass (lbm)	31.26	29.33	-6%
Burn Time (s)	4.20	4.72	+12.4%	Propellant Mass Fraction	0.32	0.43	+34%
Total Impulse (lbf-s)	1470	1864	+26.8%	Thrust-to-Weight Ratio (wet)	11.2	13.5	+15%

Table II.1. SRAD and COTS hybrid system performance and mass specifications. *Note that SRAD performance data is averaged from three test fires, two of which were incomplete burns.

The primary constraint in designing our motor was keeping the motor compatible with commercial components. As a team with little to no rocketry experience, we wanted to err on the side of caution by leaving our options open. This cross-compatibility defined the internal diameter of our oxidizer tank and combustion chamber as well as the bolt patterns that connect the two and connect to the nozzle. In past years, the UCLA team has struggled to reach ten thousand feet with the commercial motor and the thrust figures have always been lower than manufacturer's specifications. With this in mind, we decided to try to optimize the motor for ten thousand feet by increasing total impulse and thrust while decreasing dry mass. We also spent considerable effort to achieve more consistent burns by improving the fill system and ground support equipment.

To increase total impulse, we increased the length and capacity of our oxidizer tank. Previous test fires of the commercial system demonstrated that the fuel grain often regressed less than half of its radial thickness allowing us to increase burn time without risking burn-through of the fuel grain. We performed simulations using the commercial datasheet thrust curve stretched on the time axis to deliver varying total impulses. Since our motor previously underperformed, we used the commercial thrust as a conservative estimate of what we would achieve after our thrust improvements. This analysis led us to increase the capacity by 25% which was slightly oversized considering that if needed we can underfill the tank.

To increase thrust we had to increase efficiency and mass flow rate. Addressing efficiency first, we noted the most accessible improvement was to add a mixing chamber between the end of the fuel grain and the converging section of the nozzle. In a hybrid motor, fuel is being added continuously to the oxidizer and combustion gases throughout the length of the fuel grain. In the commercial system, the fuel grain extends to the converging section of the nozzle. When fuel is added to the combustion gases at the aft end of the grain, the fuel does not have enough time to mix with oxidizer and exits the nozzle as unburnt fuel. By adding a mixing chamber between the fuel grain and nozzle, a recirculation zone forms and allows a more complete burn of the propellants. The length of this mixing chamber was based on a general guideline of one-half to a full internal diameter of the motor passed down by older members of Rocket Project at UCLA. Upon researching further, there was very limited information on more exact sizing methods and due to the extremely complex processes occurring in a hybrid system, modeling the flow and combustion was infeasible.

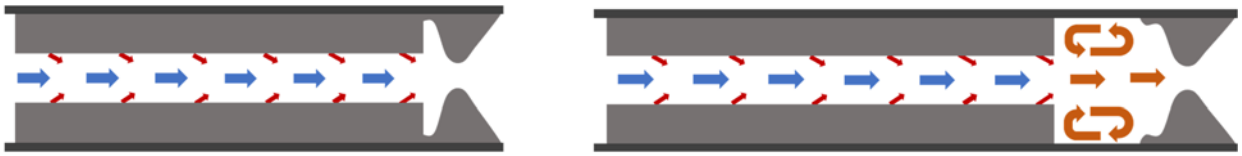

Figure II.4. Visual Representation of Combustion Chamber (a) without mixing chamber and (b) with added mixing chamber

In increasing mass flow, we were limited by our decision to use commercial fuel grains based on our mixed success in casting custom grains. The internal geometry of the grain was thus pre-determined. To preserve proper oxidizer-fuel ratios, we made no changes to the injector plate and instead would finely tune our oxidizer mass flow rate for thrust and efficiency by varying the oxidizer pressure at time of ignition. The effect of oxidizer tank pressure on thrust is displayed in the figure below of our March 3 static fire data.

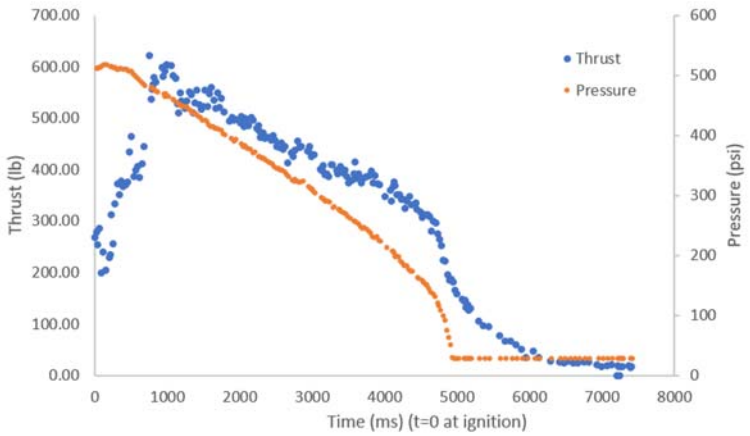

Figure II.5 March 3 static hot fire thrust & pressure data

Achieving a complete and timely fill proved a persistent obstacle to getting consistent performance. The commercial system recommended continuously venting until ignition. Our use of this system proved that losses from venting led to fill times of over ten minutes. In warm conditions where the greater vapor pressure caused higher flow rates through the vent, we were rarely able to confirm a complete fill. To alleviate this problem, we attached an electromechanically actuating valve to the vent line allowing us to intermittently vent during fill reducing losses and to close the system between fill and ignition and achieve optimal pressures via ambient heating of the nitrous oxide in the tank.

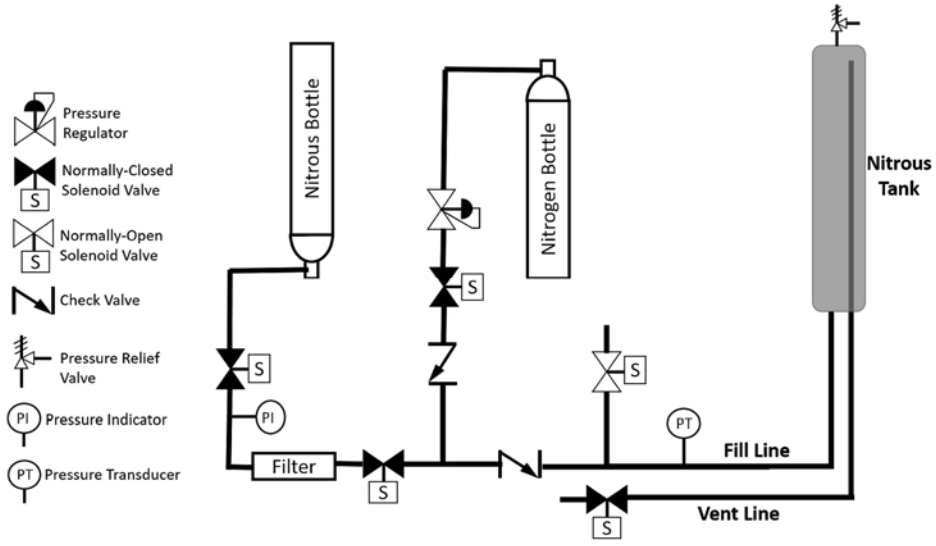

Figure II.6. Plumbing and instrumentation diagram

After adding a controlled vent, pressure control problems persisted on warm launch days along with issues of nitrous oxide becoming supercritical above 98 degrees Fahrenheit which causes low density and unpredictable behavior. The variation of nitrous oxide properties as a function of temperature is displayed bolw in Fig II.7. To alleviate this, we built a cooling system composed of packed ice around our nitrous oxide bottle to limit supply pressures to 600 psi and increase fill density. Now we are able to better control pressures to ensure safety and reliable performance.

In Fig II.6, the nitrogen tank is used for leak checks performed at 50 psi. The nitrogen pressure is then increased to 150 psi to purge the system after ignition or in case of an abort. Nominal nitrous bottle pressure is 550 psi to 650 psi and kept to this level by a bottle cooling system. During fill, nominal tank and ground plumbing pressure is 500 to 600 psi. Nominal tank pressure at time of ignition is 750 psi. The pressure relief valve at the top of the oxidizer tank is set to open at 950 psi.

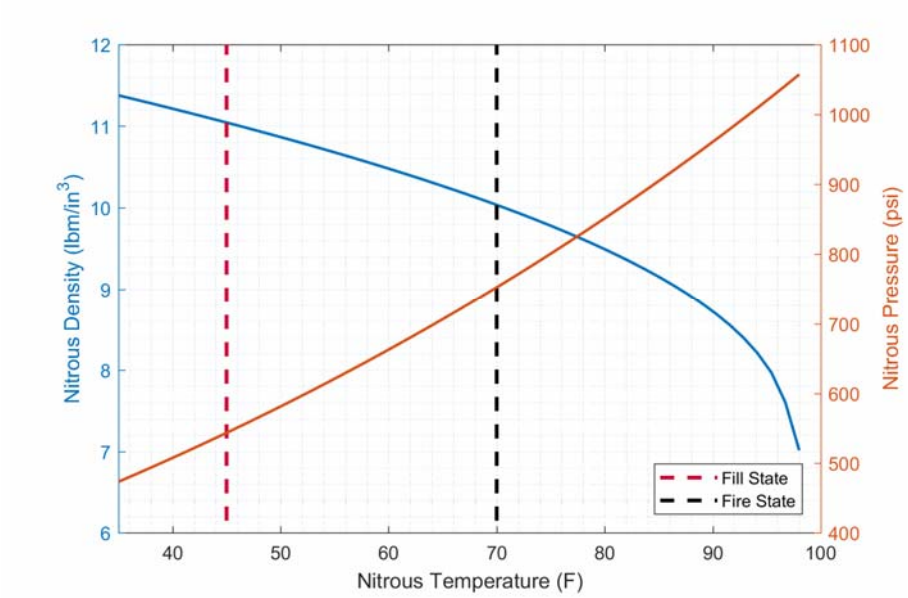

Figure II.7. Nitrous property variance with temperature; the critical point occurs at the end of this plot, 98 degrees F

Figure II.8 below shows the results of our modifications as compared to the commercial system. It is noteworthy that the March 3 test was performed at a low oxidizer pressure (~550 psi) resulting in lower than expected thrust and neither the April 15 nor the May 19 test resulted in a complete burn and therefore gave lower impulse than is expected, but thrust values similar to what we would expect. The test results are discussed further in section IV: Project Test Reports Appendix.

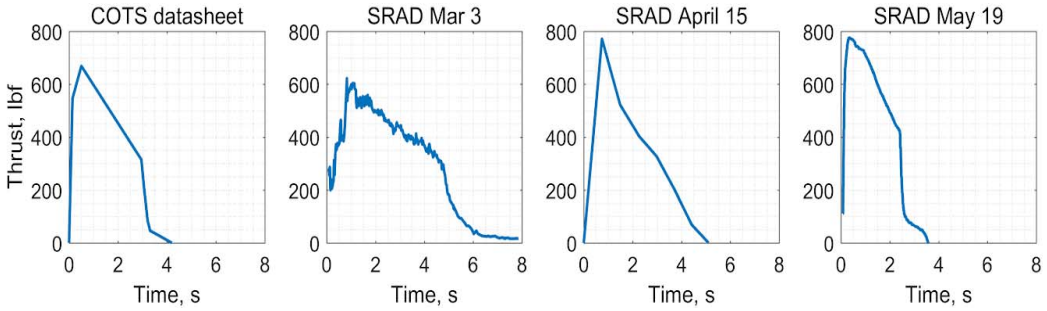

Figure II.8. SRAD static hot fire test results

In the process of manufacturing a custom oxidizer tank and combustion chamber, we were able to reduce wall thicknesses and further remove material from the end cap to minimize dry mass while maintaining a safety factor of at least 2 for all failure modes. This resulted in a 21% decrease in motor dry mass as indicated by Table II.1 above.

B. Aero-structure Subsystems

The airframe of this rocket was designed to maximize apogee and to allow for smooth integration with propulsion, recovery, and payload.

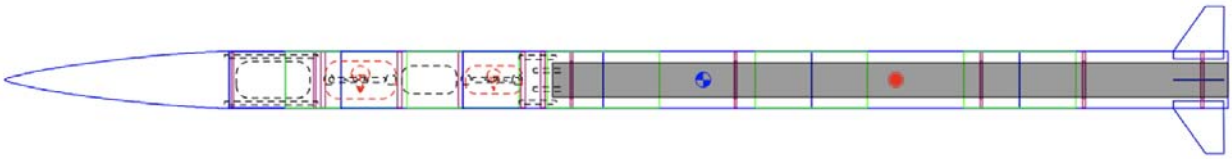

Figure II.9. OpenRocket diagram of aerostructure and internal components

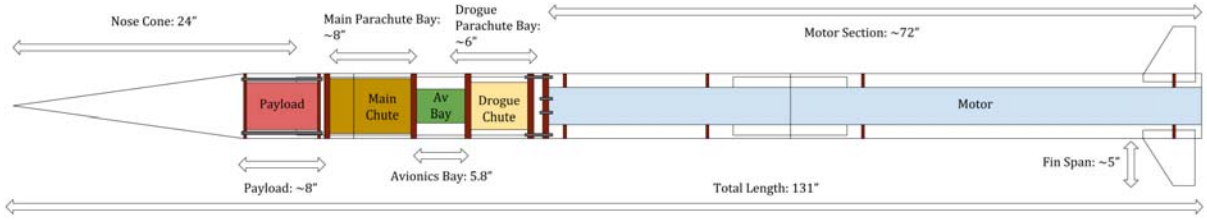

Figure II.10. Rocket length & bay diagram

Diameter (in)	6.08
Length (in)	131
Apogee (ft)	8,600
Maximum Velocity (ft/s)	856
Maximum Acceleration (ft/s^2)	401
Maximum Mach Number	0.77
Wet Mass (lbs)	58.8
Dry Mass (lbs)	46.2
Maximum Thrust (lbf)	776
Total Impulse (lbf ·s)	1760
Off-Rail Speed (ft/s)	98.4
Stability (calibers)	3.39

Table II.2: Predicted Rocket Specifications for IREC 2018.

1. Rocket Section Couplings and Breaks

The rocket is broken into four sections, plus the nose cone, to allow for parachute separation during flight and integration with the motor. Each coupler extends 6 inches on either side of the separation.

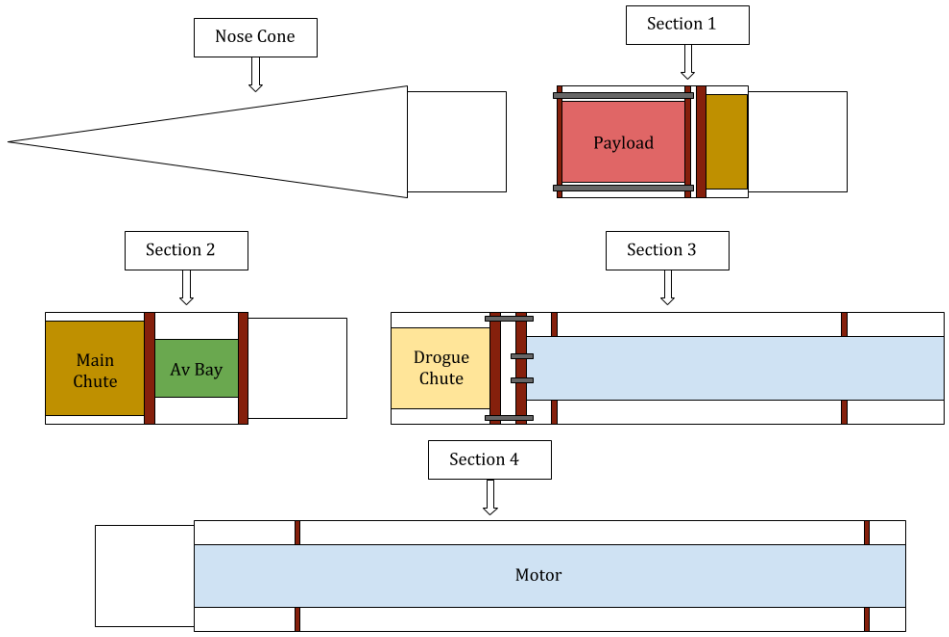

Figure II.11. Section breaks & coupling

2. Aeroshell

Hyperion's aeroshell is made out of three layers of woven pre-impregnated carbon fiber reinforced plaster (CFRP). The body tubes were manufactured by laying up 3 separate layers of the carbon fiber onto an aluminum mandrel and then curing them in an oven for 5.5 hours. Peel ply and heat shrink tape were additionally layered on top of the carbon fiber to provide compression, creating a stronger tube. Couplers were created by cutting body tubes lengthwise and then sanding the edges of the cut down to reduce the diameter of the coupler. The outer diameters of the couplers are 6 inches, while the inner diameter of the body tubes are 6 inches. The average inner diameter of the couplers is 5.92 inches, while the average outer diameter of the body tubes is 6.08 inches.

For bulkhead calculations, the equation for a circular plate that is centrally loaded was used. The thickness of the thrust bulkhead was calculated with a factor of safety of two, and the thrust used was the maximum recorded thrust for our motor. With these values, the thickness required is 0.48 inches, which for convenience of manufacturing was rounded to 0.5 inches thick.

While the thrust bulkhead takes the most force, the avionics bay bulkhead thicknesses were calculated as well. These bulkheads take the force of the parachutes deploying, so they should be checked. The same calculations were performed using that force instead of the thrust, and the thickness required was 0.35 inches, which for convenience was rounded to 0.5 inches.

The body tube thickness was calculated through force analysis. Taking into account axial stresses only, less than one layer of carbon fiber is strong enough to last the flight of the rocket. However, the body tubes needed to pressurize in order to deploy the parachutes, and one layer of carbon fiber is too porous. Three layers of carbon fiber were used to address this issue and to provide an extra level of safety.

3. Nose Cone

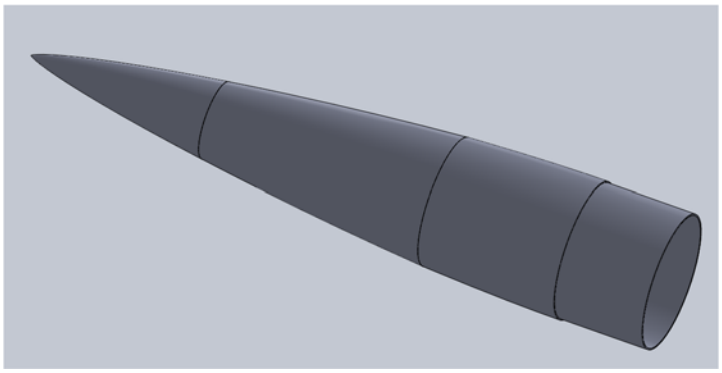

Figure II.12. Rendering of male nose cone mold which is printed in three pieces to accommodate size constraints of available printers

As the first structure to be in contact with the fluid medium, the nose cone is an especially critical part of the rocket. A lot of emphasis is placed in developing and analyzing the aerodynamic profile to ensure the nose cone does not break during launch.

The proposed design was an LD Haack profile with a fineness ratio of 4. The selection for the nose cone length to diameter ratio and profile was designed to provide satisfactory aerodynamic flow at high speeds while attempting to decrease the overall mass of the rocket. Another consideration in designing the nose cone was to accommodate the CubeSat payload.

The nose cone manufacturing procedure was decided after making two prototypes via different methods. In the first prototype, a male mold was 3D printed and then had 5 layers of fiberglass layup added over the mold to increase structural integrity and heat resistance. This method was fast and relatively simple, however, it required the male mold to remain inside the layup due to the shoulder. This added extra mass to the rocket. The second method also used a 3D printed male mold, but it was used to create two identical female molds with fiberglass. Then, a separate layup is done inside each of the female molds. When the layups are in the leather stage, the two female molds are connected to allow the two halves of the cone to bond at the seams. The first problem arose when it was difficult to ensure that the layup was made over exactly half the cone. This led to the next problem the two halves did not meet seamlessly due to gaps at the seam. This caused the two halves of the nose cone to not match up and compromised the profile of the cone. Although this purely fiberglass cone was lighter than the cone containing the male mold, the difference was not significant enough to justify the added complications and manufacturing time. Therefore, the final decision was to use the 3D printed male mold inside a fiberglass layup for *Hyperion.*

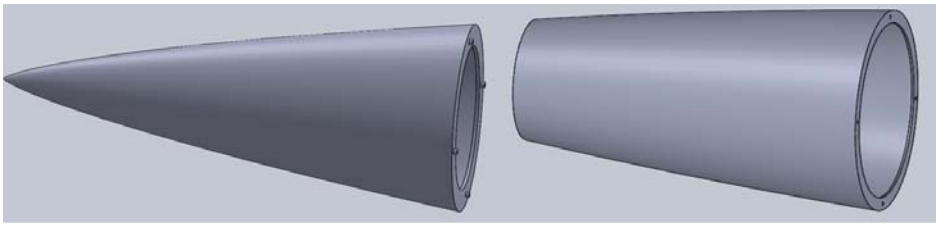

Figure II.13. First two nose cone segments as printed

At UCLA, the size of the 3D printers available to students limits what is possible to print. Because of this, the cone needed to be printed in pieces while ensuring that these pieces could be attached seamlessly. To achieve this, notches were printed that fit into corresponding divets in the shoulder of the piece above it.

4. Upper Airframe

The upper airframe of *Hyperion* consists of three sections: the payload section (section 1), the main parachute bay (section 2), and the drogue parachute bay (section 3). The payload is retained using threaded rods that will attach to a removable bulkhead. This allows the payload to be removed if needed—it can be secured directly before launch. The drogue bay also employs a removable bulkhead that is attached to the thrust bulkhead using threaded rods. This extra bulkhead will allow extra room for plumbing that will fit through a hole in the thrust bulkhead. It will also allow for pressurization of the drogue bay.

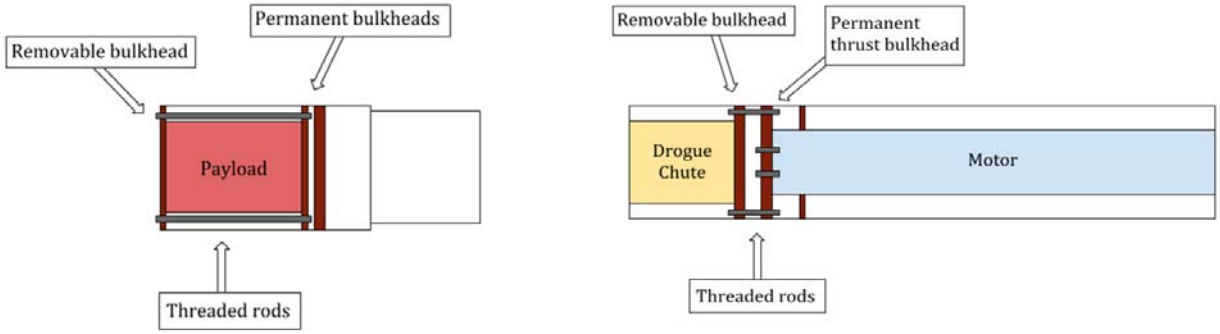

Figure II.14. Payload & recovery integration plan

To secure the motor from the top, the retainment system is based around two threaded rods that are screwed through the thrust bulkhead into the top of the motor. This method was chosen due to its simplicity, ability to hold a lot of force, and lack of restrictions on the degrees of freedom. Due to the integration of all the parts, the motor retainments main purpose is to prevent linear and rotational movement along the main axis of the rocket, with centering rings restraining all other motion. Restraining it only from the top via two rods restricts just the two degrees of freedom and is least likely to result in over constrainment. The rods have a 0.25" engagement with the motor and based on thread it can be calculated that per inch of thread there is 0.523 area of internal thread shear engagement. Considering the rod length, use of two rods, and shear strength of 6061-T6 Aluminum, the expected force that the two rods can take is 8,010 lbs which is enough to support the entire motor during any point in time of the flight. Due to this amount of strength and the desire to not overconstrain the motor this was the chosen method of retain the motor.

Figure II.15. Rendering of motor retainment system

5. Lower Airframe: Fins and Fin Retainment

The goal of our fin design team was to ensure rocket stability off-rail and throughout flight while also minimizing the drag caused by the fin structures. Since the CG shifts upward throughout the flight, the overall stability of the rocket should only increase as the flight progresses. Because of this, the point of minimum stability occurs as soon as the rocket leaves the launch rail. Prometheus utilized OpenRocket simulations as well as our own MATLAB scripts to analyze the off-rail stability provided by different fin shapes, sizes, and numbers.

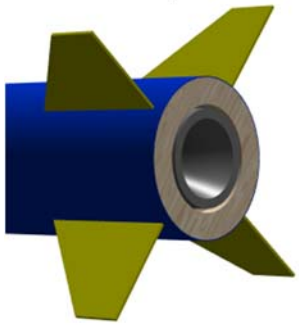

Figure II.16. Rendering of fin shape & placement

The clipped delta shape was decided upon because of its ideal combination of low induced drag and ease of manufacturing. The elliptical fin shape is the least drag-inducing shape, but it would be exceedingly difficult to manufacture. The clipped delta shape is preferred relative to a trapezoidal shape (which more closely resembles an elliptical shape) because of the back-shifted tip chord, which brings the center of pressure back more significantly per unit size when compared to trapezoidal fins.

Four fins were chosen due to their greater strength, smaller size, and ease of alignment compared to three fins. It is easier to make spare of smaller fins in case a fin is damaged. See Divergence/Flutter Analysis section for more details on strength comparison.

A carbon fiber layup was used to make the fins out of pure carbon fiber. Carbon fiber was chosen for its exceptional strength to weight ratio. The fins are made of mostly unidirectional carbon fiber laid at different angles, with the outside layers being comprised of woven carbon fiber. Then the fins are sanded into rounded airfoil into the leading and trailing edge of the fins to make them more aerodynamic. A fully tapered airfoil was considered, but it would have compromised the strength of the carbon fiber layup by sanding out most of the layers. Additionally, a fiberglass fillet will be added between the fins and body tube to further decrease the drag created by then fins.

Number of Fins	4
Root Chord (in)	5.3
Tip Chord (in)	2
Semi-Span (in)	4.8
Sweep Length (in)	3.373
Sweep Angle (degrees)	35.1
Thickness (in)	0.3
Position relative to bottom of rocket (in)	0.5
Fin Tab Length (in)	0.75

Table II.3. Fin dimensions

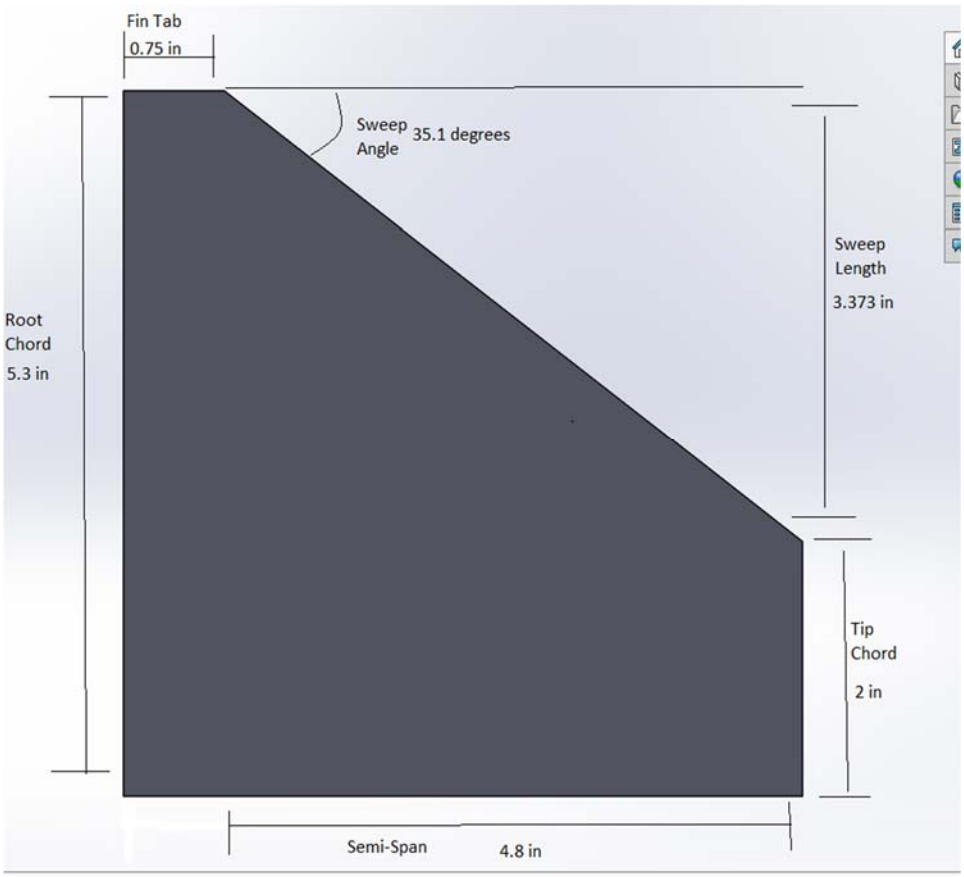

Figure II.17. Fin nomenclature with *Hyperion* dimensions.

The fin retainment system consists of two parts: a notched centering ring, and outer fiberglass fillets. Inside the body tube, there is a centering ring laser cut with 4 notches where the fins will attach to. This provides more contact surfaces between the centering ring and fin as well as more area that can be epoxied. This system gives far more retainment strength than simply epoxying the fin to the outside of the body tube. A diagram of the internal retainment system is displayed below.

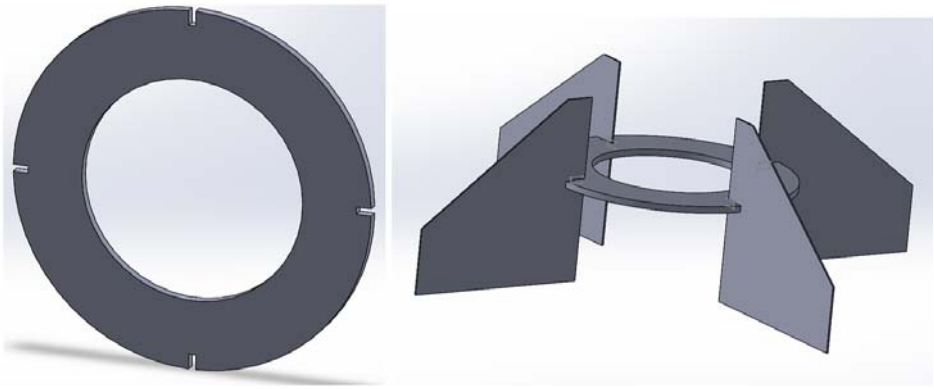

Figure II.18. Notched centering ring system for fin retainment

During integration, the fins are pushed into snug notches, then epoxied in to ensure vertical alignment and security. The system also guarantees that the fins will be evenly spaced at 90 degrees from one another. In addition, there will also be a fiberglass fillet at the fin-body tube intersection that provides additional retainment support and decreases aerodynamic drag on the fins.

Using a program called FinSim, the divergence and flutter velocities of different fin sizes were calculated. Two sets of fins were sized to give 1.5 calibers of stability off-rail, one with 3 fins and one with 4 (the 3 fin set had to have larger dimensions, creating the difference in flutter and divergence velocities). Both have the same thickness (0.3 inches). The data from the flutter and divergence simulations is displayed in the table below:

Number of fins	Divergence Velocity (ft/s)	Flutter Velocity (ft/s)	Factor of Safety
3	5631.51	7660.82	6.58
4	7333.42	9976.02	8.57

Table II.4. Fin divergence and flutter velocity. Note: maximum rocket velocity is 856 ft/s

6. Stability

The off-rail speed is a function of the mass of the rocket, the thrust of the motor, and the effective rail height which is 12.2 ft. The effective rail height is calculated by subtracting the height of the launch rail (17 ft) minus where the higher launch lug is placed (4.8 ft). We calculated our off-rail speed using an OpenRocket simulation. Therefore, obtaining the following off-rail speed:

$$V_{off\text{-}rail} = 98.4\ ft/s \tag{II.1}$$

When assuming high winds, we use the following equation to calculate the maximum angle of attack:

$$AOA = tan^{-1}\left(\frac{V_{wind}}{V_{off\text{-}rail}}\right) \tag{II.2}$$

where, V_{wind} is the wind speed and $V_{off\text{-}rail}$ is the off-rail speed. Therefore, our maximum angle of attack is expressed below:

$$AOA = tan^{-1}\left(\frac{22\ ft/s}{98.4\ ft/s}\right) = 12.6^{c} \tag{II.3}$$

Here, it is assumed that the maximum wind speed would be 22 ft/s (15 mph). Considering a slightly lower off-rail speed and slightly higher maximum angle of attack, it was decided to design the fins to be slightly larger in order to have a larger stability. This larger stability compensates for the lower off-rail speed.

Stability is a vital concept when it comes to rocketry. A stable rocket is able to correct its path when disturbed by a reasonable angle of attack. Stability is a function of the distance between the position of the center of gravity and the center of pressure. The following equation is how the stability of our rocket with respect to our body diameter was calculated:

$$Stability = \frac{X_{CP}\text{-}X_{CG}}{d} \tag{II.4}$$

where X_{CP} is the position of the center of pressure measured from the tip of the nosecone, X_{CG} is the position of the center of gravity measured from the tip of the nosecone, and d is the outer diameter of our rocket.

Hyperion's stability was measured using two different methods. The first method includes using the software program OpenRocket. The calculated stability from OpenRocket is the following:

$$Stability = \frac{95.265\ in\text{-}74.678\ in}{6.08\ in} = 3.39\ cal \tag{II.5}$$

Stability is considerably high in order to compensate for *Hyperion*'s lower off-rail speed. When considering off-rail conditions, the worst case off-rail stability is calculated from an OpenRocket simulation.

Assuming maximum wind conditions, our off-rail stability would still be approximated at 1.46 cal. Therefore, *Hyperion* still has a high enough stability margin in order to stabilize flight at the maximum angle of attack.

The second method of calculating the stability includes writing an original MATLAB script in order to calculate the position of the center of pressure and from there calculating the stability. The center of pressure is primarily affected by the geometry of the rocket, specifically the dimensions of the nosecone, fins, and body of the rocket. The body term results in the center of pressure to become a function of the angle of attack. Therefore, the following results were obtained when assuming a 0° angle of attack:

$AOA = 0°$
$X_{CP} = 97.98\ in$
$X_{CG} = 74.68\ in$
$Stability = 3.83$

When assuming the maximum angle of attack of 12.6°, the following results occur:

$AOA = 12.6°$
$X_{CP} = 83.03\ in$
$X_{CG} = 74.68\ in$
$Stability = 1.37$

Therefore, this method also yields high stability and high stability margins which creates significantly safe off-rail conditions.

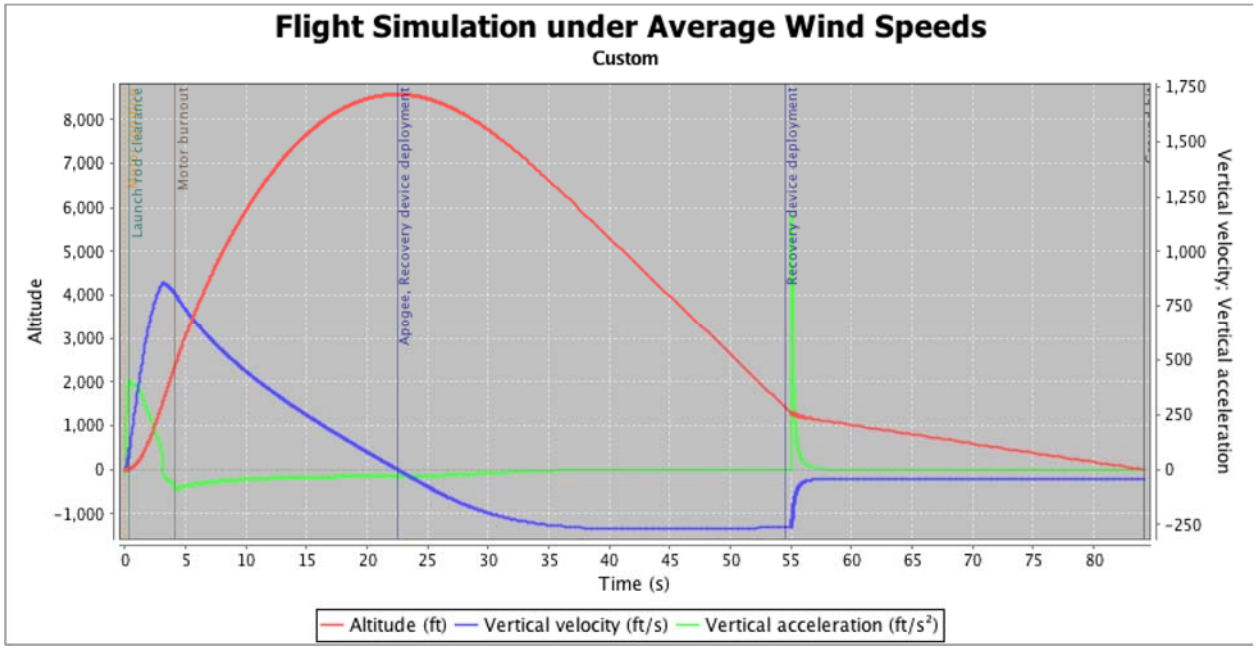

Figure II.19: Flight simulation assuming average wind speed of 13.2 ft/s (9 mph).

C. Recovery Subsystems

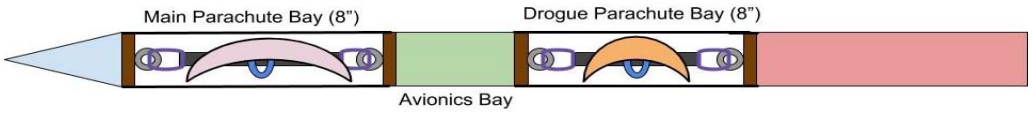

Figure II.20. Parachute & avionics bay side view

The goal of the recovery system is to safely recover the rocket and payload using a dual-deployment parachute system. The two parachutes include the drogue parachute, which will be released at apogee, slowing the rocket's descent velocity to 66 ft/s, and the main parachute, which will be released at 1500 ft and will slow the rocket's descent velocity to 23 ft/s. In order to achieve a successful recovery, the rocket will employ redundant mechanisms throughout the design. The following design elements are used: a 3D printed avionics bay that houses two barometric altimeters (Stratologger CF) powered by two 9-volt batteries (wired as independent circuits for redundancy), four Peregrine CO2 ejection systems, which will release 24 grams of CO2 for the drogue parachute bay and another 24 grams of CO2 for the main parachute bay, a 36" diameter drogue parachute with a 25' drogue shock cord, a 84" diameter main parachute with a 25' main shock cord. The system, seen in Figure II.19, is laid out in the following manner: the drogue parachute bay sits above the main thrust bulkhead, the avionics bay sits above the drogue parachute bay, and the main parachute bay sits directly above the avionics bay. Each bay is vacuum sealed using a mix of Epoxy and vacuum-rated tape to prevent pressurization leakage.

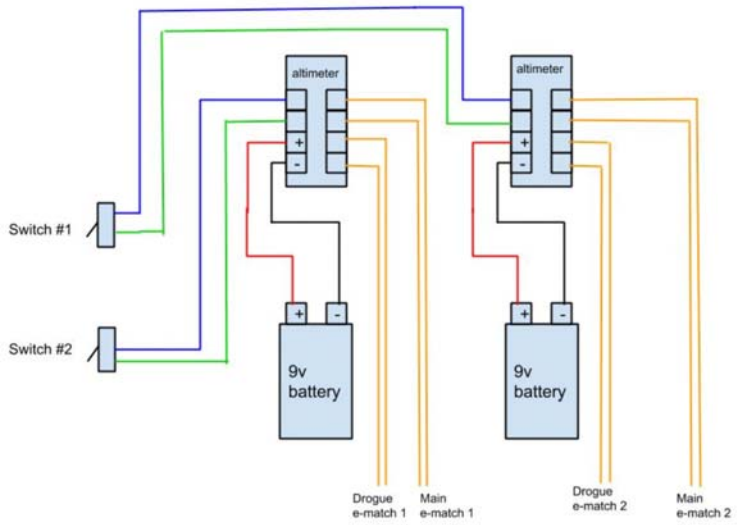

Figure II.21. Redundant recovery system wiring diagram

The parachutes' diameters and shock cord lengths were carefully selected to follow IREC regulations and to minimize chances of damaging the rocket. For the drogue parachute, we selected a parachute such that was big enough such that the rocket was at a safe velocity for main parachute deployment, yet small enough in order to minimize drift in the air, to reduce shock in the case of any horizontal velocity at apogee, and to reduce the overall weight of the rocket. Using a MATLAB script developed by Rocket Project at UCLA we were able to simulate the descent velocity and impact energy for based on the mass of the rocket. Using this simulation, we selected the 36" Fruity Chutes Classic Elliptical Parachute as it struck a perfect balance between these requirements and has worked well in previous years of UCLA Rocket Project (such as last year's Hydra Rocket). For the main parachute, we needed a parachute that was large enough to ensure that our rocket would minimize impact energy in order to minimize damage to the body tube sections upon landing. However, we wanted the parachute to be small enough to reduce drift, minimize shock upon deployment, and to reduce the weight of the overall rocket. Our desires were satisfied by our choice of the Fruity Chutes 84" Standard Iris Ultra parachute. We calculated an impact energy of 456.40 lb-ft upon landing, which based on Rocket Project precedent, is far below the impact energy required to prevent damage to the rocket structure.

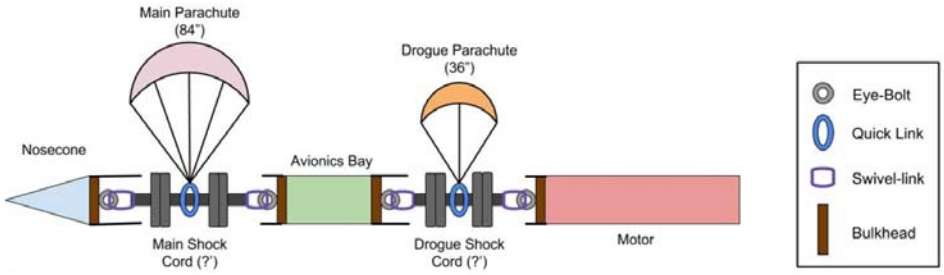

Figure II.22. Parachute connection & sizing diagram

Shock cords were selected according to several desired factors. Mainly, we wanted a shock cord that would be strong enough to endure the shock upon parachute deployment, yet small enough to minimize unnecessary weight. Using another MATLAB script developed by Rocket Project at UCLA we were able to simulate shock load based on shock cord length as seen in Figure II.22. We selected ⅜" Flat Webbing Shock Cord from Fruity Chutes, tested up to 1000 lbf. According our calculations, this is far above our maximum expected shock force of 200 lbf, which will ensure safe operation even in the event of higher shocks than expected (as in the event of extra horizontal velocity at apogee). As for selecting the length of shock cords, our top priorities were to have cords long enough to minimize the shock on the cord and airframe and to prevent body tube sections from impacting each other in the air upon parachute deployment. The figure below shows that the selected shock cord lengths satisfy the clearances required to prevent impact between body tube sections, even in the event of oscillations following parachute deployment. Additionally, our analysis of varying shock cord length and its effect on the shock during deployment indicates that our selection of a 25' cord significantly minimizes the shock as desired.

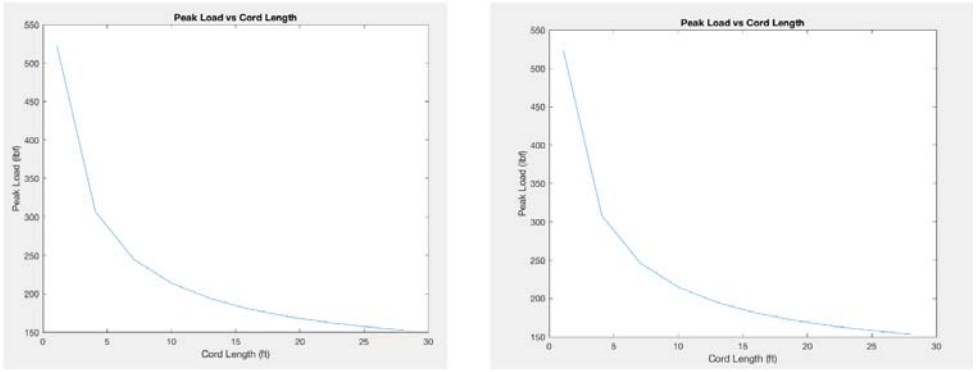

(a) (b)

Figure II.23. Shock cord length vs. peak load for (a) drogue and (b) main parachutes

Finally, the issue of zippering of body tube sections posed to be an in issue in the past of UCLA Rocket Project. We addressed this issue this year by moving the separation point in the body tube closer to the aft of the rocket, such that upon parachute deployment, the shock cord will not put significant stress on the side of the body tube section.

The avionics bay structurally consists of two 3D printed pieces and a ¼" steel rod with eye nuts on each side. Inside the bay lies the heart of the recovery system: a redundantly wired avionics system which will pressurize the parachute bays to deploy the parachutes.

Figure II.24. Rendering of 3D printed avionics bays

At apogee, the altimeters will detect a change in barometric pressure and will send a current through e-matches contained in two charge cups beneath the 12 gram CO2 canisters. This will ignite the two 0.2 gram black powder charges, driving the canisters in a sharp pink, causing 24 grams of CO2 to flood into the drogue parachute bay. The CO2 pressure (approximately 790 lbf exerted on the bay) would break four shear pins (approximately 49 lbf for each sear pin to break) and will cause a separation in the body tube sections at the drogue parachute bay, thus releasing the drogue parachute and shock cord.

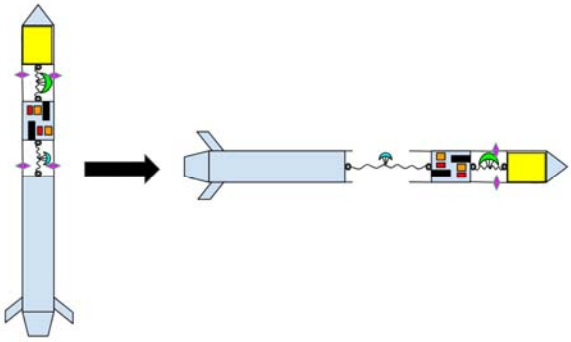

Figure II.25. Recovery system at drogue deployment

The rocket will descend with an inflated drogue parachute at a descent velocity of 66 ft/s. At 1500 ft, the altimeters will send a current through e-matches into the second group of CO2 ejection systems, thus igniting 0.2g of black powder, and allowing 24g of CO2 to pressurize the main parachute bay. This will break 4 more shear pins, causing a body tube separation at the main parachute bay, thus releasing the main parachute and shock cords. Following main parachute inflation, the rocket will descend at 23 ft/s until it impacts the ground.

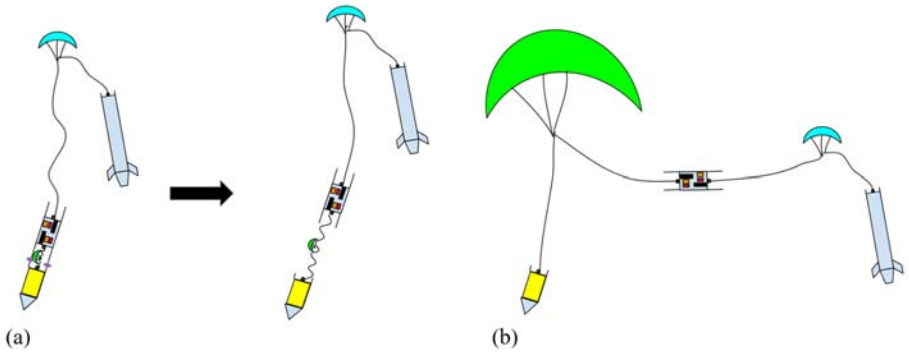

Figure II.26. Recovery system at (a) main deployment and (b) landing

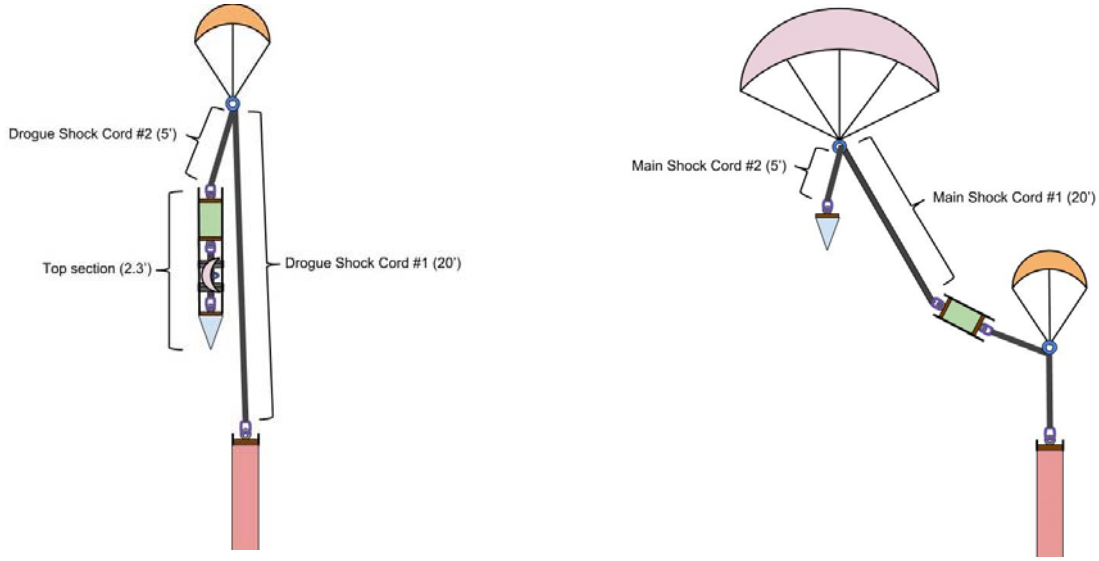

Figure II.27. Shock cord lengths during drogue deployment and main deployment

D. Payload Subsystems

The goal of the payload, modeled after the CubeSat standard, is to acquire and transfer telemetry data in-flight and store data for post-flight analysis. The payload needs to successfully integrate with the rest of the rocket and perform the necessary data collection and telemetry tasks.

1. Structure

The SensorTile is the main data collection module on the payload. The sensors on the SensorTile include a gyroscope (in an x,y,z format), an accelerometer (with a range of +/-16g and an x,y,z format), and a magnetometer (also in a x,y,z format). In-flight data collected from the SensorTile will be stored on an SD card for post-flight recovery.

Timestamp	AccX [mg]	AccY [mg]	AccZ [mg]	GyroX [mdps]	GyroY [mdps]	GyroZ [mdps]	MagX [mgauss]	MagY [mgauss]	MagZ [mgauss]
00:14.3	27	23	1022	210	-1330	1610	292	-703	-277
00:14.4	28	20	1021	280	-1330	1540	289	-702	-283
00:14.5	32	26	1021	280	-1330	1610	289	-691	-282
00:14.6	24	22	1019	280	-1260	1540	295	-705	-273
00:14.7	29	26	1019	210	-1330	1610	292	-694	-274
00:14.8	30	22	1022	280	-1330	1610	291	-705	-277
00:14.9	30	23	1022	280	-1260	1610	288	-705	-279
00:15.0	25	23	1021	280	-1330	1610	294	-700	-285
00:15.1	26	30	1021	280	-1260	1610	288	-697	-285

Figure II.28. Sensor tile sample data

The GPS coordinates will be transmitted to the ground system via a LoRa radio. Two trained members will be present at the ground system computer to monitor the status of the payload and telemetry system and troubleshoot if necessary. Once received by the ground system, the GPS data will be saved to a text file which will be analyzed along with the other data after the SD card has been retrieved from the rocket. Both the SensorTile and the telemetry system will be powered by two separate LiPo batteries, seen in Fig II.29.

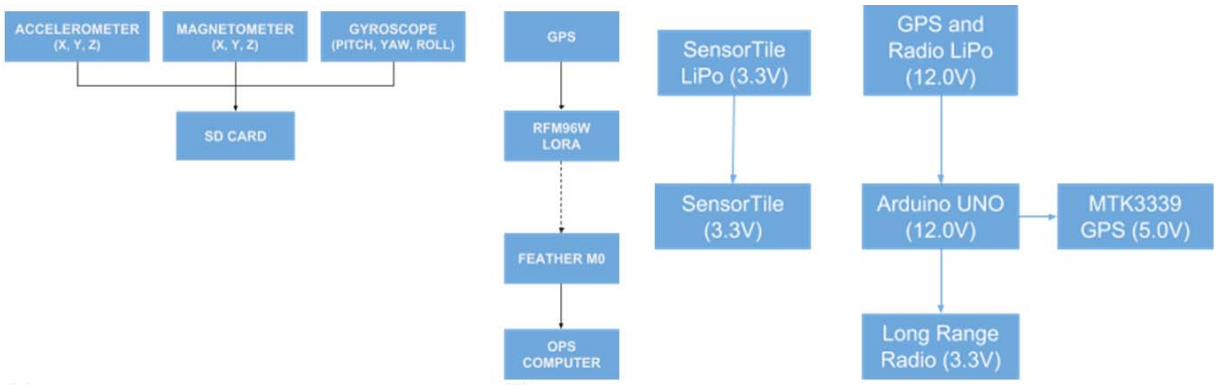

(a) (b)

Figure II.29. In-flight (a) data transmission and (b) power flowcharts

Component	Quantity	Unit Mass (lb)	CBE (lb)	Margin	CBE - Margin (lb)
Arduino Uno	1	0.0551155	0.0551155	15	0.0001397350437
Ultimate GPS	1	0.01873927	0.01873927	15	0.00004750991484
SensorTile	1	0.0220462	0.0220462	15	0.00005589401746
Lipo Battery (ST)	1	0.010251483	0.010251483	15	0.00002599071812
Lipo Battery (Arduino)	1	0.551155	0.551155	15	0.001397350437
Antenna	1	0.03747854	0.03747854	15	0.00009501982968
LoRa Radio Transciever	1	0.006834322	0.006834322	15	0.00001732714541
	CBE (lb)	CBE - Margin (lb)			
TOTAL COMPONENT MASS	0.701620315	0.001778827106			
CHASSIS MASS	6.6	7.59			
TOTAL PAYLOAD MASS	7.301620315	7.591778827			
BOILER PLATE MASS	1.5	1.725			
TOTAL MASS	8.801620315	9.316778827			

Table II.5. Payload mass budget

2. Data Analysis

The goal of the data analysis is to get an approximate location of the payload using the Inertial Measurement Units (IMU) data (magnetometer, gyroscope, and accelerometer).

The integration of the gyroscope and magnetometer values produces the actual angles of the orientation of the rocket, thus providing the roll, pitch, and yaw values of the rocket. The magnetometer provides the constant reference frame (magnetic north) to compensate for the gyroscope drift that may appear after integration. The accelerometer values can be integrated to provide velocity, or the change in position. Again, there is a velocity drift resulting from the integrated accelerometer data. To compensate for this drift, a Kalman filter algorithm can be used to estimate the actual change in positions of the rocket. The relative position, then, can be found by combining the initial longitude/latitude of the payload to obtain an actual longitude/latitude value of the final position of the payload.

The significance of this data is that IMU's are commonly used for navigation purposes and the fusion of these three sensors is optimal for reducing drift related errors that are a typical problem when trying to obtain the most accurate position values.

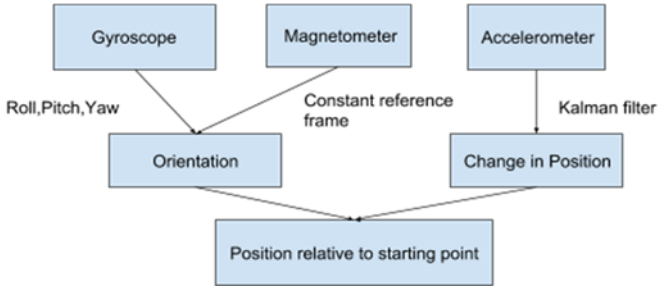

Figure II.30. Post-flight data analysis flowchart

III. Mission Concept of Operations Overview

A. Definition of Electrical Modules

The following modules are used in preparation for the rocket's launch:

1. *Control Module*
   The control module consists of the control circuits and the live data feed system. All communication between the launch pad and the control module is via a wired analog connection for reliability and simplicity. The control circuits are wired directly into the solenoid and ignition relay circuits. The live data feed system receives analog voltage signals from launch pad sensors and processes them for post-fire analysis and live display during fill.

2. *Propulsion Interface Module*
   The propulsion interface module houses the control relays, the circuitry for data system amplification and the properly regulated power sources for each of the control and data systems.

3. *Avionics Telemetry System*
   This system is composed of a radio module onboard the launch vehicle, a ground antenna that communicates with the launch vehicle, and a ground operations laptop that receives and process the telemetry data.

4. *Recovery module*
   The recovery module is composed of the two parallel systems of altimeters, e-matches, arming switches, ejection charges and power sources that are responsible for altitude detection and properly timed recovery system deployment

B. Briefing with Range Safety/Firing Officers

Upon arrival at the launch site, the avionics and propulsion control leads must coordinate a briefing with the Range Safety and Firing officers before beginning any pre-launch setup. This meeting is necessary to determine the location of the launch rail and command center as well as the radio frequencies in use by competition organizers to avoid radio interference.

C. Pre-launch Setup & Component Verification

Once the designated launch rail and control centers are determined, the analog cable connecting the propulsion interface and control modules will be run between the two sites. Simultaneously, the data processing portion of the control module will be setup for live data displays.The interface module will be connected to the solenoid valves and instrumentation. The avionics telemetry system will also be powered on and checked to ensure proper vehicle-to-ground communication. After the avionics system is checked, it will be incorporated into the airframe and we can load the rocket into the launch rail.

Once propulsion control and interface modules are wired, we will power the interface module first checking that each battery is in a nominal state of 12V or greater. We will perform a control and valve check as detailed in Appendix IV to ensure proper communication and valve actuation. Data acquisition systems will then be checked that they are detecting ambient conditions. At this point all controls, data acquisition, and telemetry systems are in nominal states.

D. Propulsion System Leak Checks & Fill

Once all electrical systems are nominal, all non-essential personnel will be cleared from the launch pad and the propulsion team will commence leak checks of the system. There will be a control operator at the command center responsible for sending control signals to the interface box. At the launch pad, a designated team member in proper PPE will be responsible for opening the supply bottles, monitoring pressures, and making final visual and auditory checks of the system. The team will announce to the officers that final leak checks and fill are about to begin. Once proper announcements are made and the area is cleared, checks and fill will begin.

The control operator will arm "Control PWR" allowing for the actuation of valves and ignition on the launch pad. At this point, ignition cannot occur: the ignition leads will be disconnected from the interface box on the pad and the team member on the launch pad will be in possession of the key needed to arm the ignition safety on the control box. The control operator will then perform the low pressure leak check as detailed in Appendix IV. Once complete, the control operator will disarm "Control PWR." The launch pad personnel will connect and secure the ignition leads. At this point leak checks are complete and the system is nominal if no leaks are present. Launch pad personnel will return to the command center and fill may commence.

E. Fill and Fire

At this point, our team will give the "READY" signal to the Range Safety/Firing Officers indicating that we are ready to begin the fill and fire sequence for our hybrid rocket system. The team will wait for the officers to announce the intention to launch and ensure the area is cleared. Once the Range Safety/Firing Officers give the "CLEAR TO PROCEED" signal, the team will initiate the fill and fire sequence. The control operator will arm "Control PWR" and proceed will the fill procedure as detailed in Appendix 2.

F. Mission Events

Once fill commences, the first phase transition occurs when the tank is filled. The tank is considered full when a white plume is confirmed visually via binoculaurs or a remote camera, the proper oxidizer mass is detected via a load cell measuring the rocket mass during fill, or by operator readings of pressurization data during vent cycles. At this point the system is closed for pressurization.

Pressurization is achieved when the pressure data reads our nominal ignition pressure of 750psi. At this point, the ignition sequence begins.

In rapid succession: ignition is confirmed by smoke and flame exiting the nozzle; liftoff is confirmed by the first upward movement of the rocket; launch rail clearance is confirmed when the upper launch lug clears the top of the launch rail. The nominal state at this point is that the rocket is continuing in a stable and straight trajectory.

The next major flight event is apogee which will occur when the rocket reaches its maximum height and begins to fall down. Simultaneously, the drogue parachute should deploy. Nominal conditions are achieved when the rocket is descending under parachute. This will be confirmed visually. When the rocket reaches 1500 feet, the main chute should deploy and deployment should be visually confirmed. When the rocket reaches the ground, landing has occurred.

IV. Conclusion & Lessons Learned

Throughout this process, we repeatedly saw how important it is to allow time for unanticipated issues. Despite our best planning and efforts, problems will always arise during manufacturing and integration that require substantial time to analyze, redesign, and remanufacture. Notably, we experienced significant challenges with our carbon fiber layup process. We learned that the storage methods have a drastic effect on the properties of the material and that different types of carbon fiber are more brittle than others. Another challenge we faced was in integration. For example, the challenge of fitting bulkheads over the motor bolts. This taught us how important it is to communicate between subteams about our respective designs and how they will affect each other's manufacturing processes. One of the most beneficial projects our team did in preparation for this competition was creating two different test rockets. This allowed us to experiment and perfect many of our manufacturing techniques before beginning our competition rocket.

Throughout the design and manufacturing process, the airframe team learned how to solve unforeseen problems as they came up. Organization and team management became very important for the team, because communication with team members and with other subteams (i.e. propulsion, avionics) was critical. The airframe team employed new techniques such as laser cutting bulkheads and centering rings and performing fiberglass layups (for the nose cone). We also successfully integrated a camera in their smaller test rocket *Hercules*—something Rocket Project had never done before. The biggest problems faced were during the carbon fiber layup process as well as the integration process. Carbon fiber is a finicky material and changes drastically depending on its age and how carefully it is stored at the proper temperatures. We experienced brittle, dry carbon fiber that did not cure to a strong enough product. Because of this, new carbon fiber had to be acquired and the layup process had to be altered. Overall, as a team full of new members, each person learned a multitude of manufacturing processes in addition to gaining theoretical knowledge to justify design and manufacturing designs.

A lot was learned during the development of our recovery system. Through one failed recovery attempt on our first test rocket we learned the important of testing. This changed our approach to developing iterations of our systems and eventually our competition system. Additionally, throughout iterations of the avionics bay we developed from a machined wooden bay to a 3-D printed bay with parts specially selected to reduce shock load. With each iteration also came improved wiring efficiency. The main takeaway from our experience was the value of testing and iteration of design.

The design and manufacturing of the individual parts to contribute to the Student Research and Design category for IREC was a particularly difficult challenge, especially for the first-years on the team who had little to no experience with such tasks. A lack of experience with the software added the challenge of learning which tool to use for the job, how to best approach a problem to solve it quickest, and even where to find particular tools on the user interface itself. In addition, new members quickly learned that the design process is more than being given a set of strict dimensions and constraints to construct a computer model. Design begins with few constraints, and considering how the part will be manufactured, changes specifications and the design itself. The team learned this best when considering where to place holes on the injector plate, only to realize that the plate had to be moved since we would need to bore out the piece from a single aluminum piece rather than welding due to our resources. The team also learned that the design process is often the quickest part of the task, and that manufacturing is a monumental challenge in itself. Many hours of machining were needed: properly setting up the piece on the lathe, determining the best way to go about a cut, and performing the cut itself. The team also learned that the smallest mistake can have the largest consequences when it comes to manufacturing, and although the part does not have to be perfect—because perfection itself is hard to achieve—every maneuver matters, and constant concentration and safety are key. Even though the student-designed coupler piece will not be used for the competition motor configuration and it has still never tested due to a lack of time, it gave the team valuable experience in the design and manufacturing process.

Beyond the design and manufacturing process, the propulsion team learned about the value of high-level tests. Having data acquisition and ground plumbing components properly prepared and tested before beginning tests was paramount to test success. Attempting test fires was the most valuable experience to refining our system as one day at the desert test site would uncover more difficulties than we could anticipate in a week of discussion. The propulsion team to the best of their ability took on the method of testing often, failing often, and testing again to increase iteration speed and learning. This culminated in the simple realization that nothing will ever be perfect the first time, but that it is also nearly impossible to predict what exactly won't work without proper testing.

Appendix I: System Weights, Measures, & Performance Data

Overall rocket parameters:

	Measurement	Additional Comments (Optional)
Airframe Length (inches):	131	
Airframe Diameter (inches):	6.08	
Fin-span (inches):	15.08	
Vehicle weight (pounds):	37.2	
Propellent weight (pounds):	12.6	
Payload weight (pounds):	9	
Liftoff weight (pounds):	58.8	

Number of stages:	1	
Strap-on Booster Cluster:	No	
Propulsion Type:	Hybrid	
Propulsion Manufacturer:	Combination	Our motor will be comprised of a custom ox tank, custom ox tank end cap, custom cumbustion chamber, as well as a commercial graphite nozzle insert and retainer, commercial injector plate/coupler, and commercial solid hybrid HTPB grain. The commercial components are all manufactured by Contrail Rockets.
Kinetic Energy Dart:	No	

Propulsion Systems: (Stage: Manufacturer, Motor, Letter Class, Total Impulse)

1st Stage: SRAD Hybrid, 1.67 pounds of HTPB-Paraffin propellant and 10.93 punds of Nitrous Oxide, M class, 7,828 Ns

Total Impulse of all Motors: 7,828 (Ns)

Predicted Flight Data and Analysis

The following stats should be calculated using rocket trajectory software or by hand.

Pro Tip: Reference the Barrowman Equations, know what they are, and know how to use them.

	Measurement	Additional Comments (Optional)
Launch Rail:	ESRA Provide Rail	
Rail Length (feet):	17	
Liftoff Thrust-Weight Ratio:	6.19	

Launch Rail Departure Velocity (feet/second):	98.4	This is the reason we have such a high static margin. We also may be slightly thinning our tank, which will put our off the rail speed above 100 ft/s. Additionally, we have done matlab simulation work to ensure that our vehicle will be safe exiting the rail at this speed.
Minimum Static Margin During Boost:	3.39	*Between rail departure and burnout
Maximum Acceleration (G):	12.46	
Maximum Velocity (feet/second):	856	
Target Apogee (feet AGL):	10K	
Predicted Apogee (feet AGL):	8,600	

Payload Information

Payload Description:

Our payload will be a data acquisition device which will gather in-flight data to assist our team in future rocket design. Its main objectives are to collect, store, and analyze data about the rocket's trajectory and external environment. The sensors, which include an accelerometer, magnetometer, gyroscope, thermometer, barometer and GPS module, will be wired to an Arduino microprocessor which will store data for processing post-flight. We will use the CubeSat model if the final diameter is greater than 6 inches, and the NanoSat model if it is smaller than 6 inches. This diameter determination will be made within the coming weeks as we work to better analyze the data from our first static fire of our SRAD configuration.

Recovery Information

Our recovery and avionics bay will be using two StratoLoggerCF altimeters wired in parallel to allow for redundancy. Each will be connected to the CO2 charges held in aluminum at both the top and bottom bulkheads that contain the bay. When triggered by the altimeters, a small ematch will ignite a small amount of black powder inside the container that will push the charge cup and cause the CO2 to release, pressurizing the bay. There will be both a drogue and main parachute each in a seperate bay.

Planned Tests

* Please keep brief

Date	Type	Description	Status	Comments
1/20/18	Ground	Static Fire #1 of COTS M1575 Motor	Successful	Gathered data needed to make custom modifications
2/3/18	In-Flight	Launch of Avionics Test Rocket	Successful	Tested a scaled down version of our dual-deployment recovery system
3/3/18	Ground	Static Fire #1 of SRAD Hybrid Motor	Successful	Roughly 150% of commercial system's impulse was achieved
4/15/18	Ground	Static Fire #2 of SRAD Hybrid Motor	Successful	Data sampling rate was low; fire was successful.
5/19/18	Ground	Static Fire #3 of SRAD Hybrid Motor	Successful	Sufficient initial thrust for stable liftoff and off-the-rail speed confirmed
6/2/18	Ground	Static Fire #3 of SRAD Hybrid Motor	TBD	We will be firing one more time before competition to further ensure reliability

Any other pertinent information:

Over the course of the project, our capabilities have changed, and so we were able to manufacture more custom components for the redesigned Contrail M-1575 system which we have been using. Due to limited testing opportunities, however, we will only be using custom tanks (Ox-tank and combustion chamber), a custom graphite nozzle insert, and a custom ox tank end cap. The fuel grain, injector plate/coupler, and nozzle retainer will all be commercial.

Our team is made up of all first-year members of the club, with the exception of the project lead. Despite the relative inexperience of the team, we have come a long way and been able to make major improvements to the same hybrid system that was used by our team in past years. Such improvements include improvements to the nitrous oxide filling system, increasing the ox-tank capacity, and adding a post-combustion chamber to the combustion chamber. Thanks to these changes, we have been able to achieve roughly 180% of the total impulse that was recorded for our team in previous years with the commercial system.

Appendix II: Project Test Reports

A. Recovery Testing

Testing of the rocket's recovery system comes in the form of two main methods. The first method ensures that the altimeters and the ignition of the e-matches is working correctly. To operate this test, we remove the avionics bay from the rocket and remove the ejection tubes from the avionics bay. We wire the e-matches to the altimeters, and place the entire avionics bay into a vacuum-chamber. We then arm the altimeters, and remove ourselves from the immediate vicinity. The pressure in the vacuum chamber is removed (pump indicates a removal of 15 psi), and we shut off the pump such that air leaks back into the chamber. Immediately, the altimeters should detect a change in barometric pressure and sense that the rocket is at apogee, thus sending a signal to the drogue parachute ematch. Confirmation of the e-match ignition can be heard from outside the chamber. After another 10 seconds, the altimeters should likewise ignite the main parachute ematch. Again, confirmation of e-match ignition can be heard from outside the chamber.

The second test ensures that the rocket structures are separating correctly. This time, we load the ejection tubes in the avionics bay, and place them in the rocket. Instead of relying on the internal altimeters (which have been verified to be operating nominally in the previous test), we rely on an external altimeter in a vacuum chamber. We assemble the rocket, screw in the shear pins, and wire the ematches from inside the rocket to the altimeter inside our vacuum chamber. The rocket is strapped down horizontally to a testing cart, and is placed in a field such that the rocket components will not damage anything or be damaged. We step back to a safe distance. We repeat the vacuum pump procedure as outlined in the previous test. Once the pump is shut off, we should observe an ejection charge firing and a separation in the middle of the rocket. We should also observe the parachute and shock cord being launched out of the parachute bay. This indicates that the shear pins have broken nominally and that deployment of the drogue parachute is working. After about 10 seconds, the same should occur for the main parachute.

Using this combination of tests verifies that our recovery system, including its electronics and physical components, is operating as it should.

B. Propulsion Testing

In February 2018, a hydrostatic test was performed of the SRAD combustion chamber and oxidizer tank. The oxidizer tank has a maximum expected working time of 10 minutes and was kept at pressure for 25 minutes for one cycle followed by two 10 minute cycles. The combustion chamber has a maximum expected working time of 8 seconds and was tested through three 5 minute cycles. No leaks or deformations were detected.

	Oxidizer Tank	Combustion Chamber
MEOP	300.	850.
Hydrostatic Test Pressure	450.	1275
Theoretical Burst Pressure (FS)	1320 (4.4)	1785 (2.1)

Table A2.0.1. Pressure vessel design & test pressures (all values in psig)

The first static hot fire of our system was completed on March 3. Our first fire attempt resulted in a disconnected fill line just before ignition prompting a full purge of the system. The second hot fire attempt resulted in a full fill and fire of the SRAD motor. Due to low ambient temperature, the oxidizer pressure was lower than optimal resulting in lower than optimal thrust, but higher than anticipated burn time and total impulse.

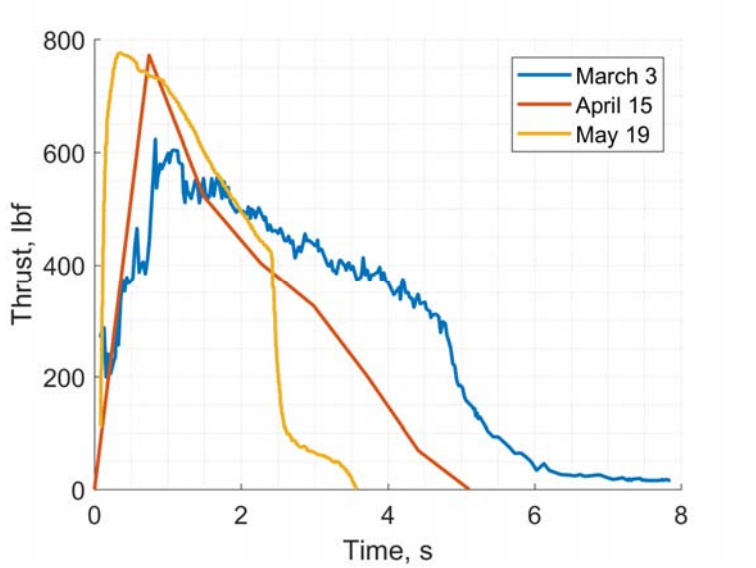

Figure A2.0.1. Static hot fire thrust curves

On April 15, we completed a second static fire of our SRAD system. Between the March and April tests, we thinned the walls of our oxidizer tank and combustion chamber to reduce motor mass and performed hydrostatic pressure tests following the same standards as those described previously. At the time of this test our fill system was unrefined and we had no confirmation of a full fill. We fired the motor at 800 psi, slightly above our optimal pressure and achieved expected thrust. The impulse was lower than optimal due to the incomplete fill. Our maximum thrust was measured as being consistent with thrust required for safe off-the-rail speed. Our data acquisition system during this test partially malfunctioned causing a low sample rate and insufficient data to accurately model rocket flight.

A third static fire was completed on May 19th. Our fill and fire procedures were refined allowing a sub-five minute fill and ignition at 750 psi. The burn ended prematurely for this fire as well. The thrust was as expected and consistent with April 19 data. Once again, off-the-rail speed requirements were met. Total impulse was lower than optimal resulting in a sub 10k foot apogee but ensuring a safe launch vehicle.

	March 3	April 15	May 19
Avg Thrust (lbf)	369	332	484
Max Thrust (lbf)	622	771	775
Burn Time (s)	5.9	5.1	3.2
Total Impulse (lbf-s)	2171	1698	1536

Table A2.0.2 SRAD static hot fire data

Appendix III: Hazard & Risk Analysis

A. Failure Mode, Effects and Criticality Analysis (FMECA) Value Legend

	Severity	**Likelihood**	**Detection**
1	Minor inconvenience	Remote	Obvious
2	Inconvenient	Unlikely	Notice during inspection
3	Minor project setback	Likely/has happened before	Notice only during thorough inspection
4	Major project setback/ personnel discomfort	High chance	Unlikely to detect
5	Serious injury to people	Almost guaranteed	Not detectable until failure

B. Transit and Preparations

Hazard	**Failure Cause**	**S**	**L**	**D**	**R**	**Control Method**
Hybrid fuel grain burns in transit or storage	Accidental ignition of other energetic nearby or presence of oxider and ignition source	5	1	4	20	Fuel grains are stored separately from energetics and oxidizers
High pressure supply bottle damage and rapid depressurization	Forceful impact on unprotected valve block	5	1	2	10	Supply bottles will be properly secured, regularly checked, and always transported with proper safety caps in place
Skin or lungs exposed to fiberglass dust	Work cutting and sanding fiberglass brings personnel in contact with fiberglass particles	4	3	3	36	All fiberglass work will be done in proper PPE: coat, gloves, and an N95 face mask

Carbon Fiber splinters embed themselves in skin	Body tubes crack or ends are not properly finished	4	4	2	32	Team members will handle carbon fiber components with care and using proper PPE. All splintered regions will be sanded.
Eletrical Shock	Wiring can be unexposed during equipment handling	4	3	2	24	Insulation will be installed on all possible connections. Power sources wil be disconnected before work is done on electrical components.
Accidental deployment of CO_2 charges	Pressure changes due to work on body sections can trigger deployment	4	2	4	32	Recovery system will be disarmed at all points until ready for fill and fire

C. Final Assembly & Checks

Hazard	Failure Cause	S	L	D	R	Control Method
Short circuit results in premature ignition while personnel near rocket	Careless handle of ignition circuitry	4	2	4	32	Ignition leads are the last component connected before fill. Ignition without nitrous oxide would result in non-energetic flame
Explosion or rupture of oxidizer tank causing injury to personnel	Overpressurization of nitrous oxide or flaws in tank material	5	3	3	45	Tank roperly pressure tested, relief valve and normally open dump valve in place. No nitrous enters system until ALL personnel evacuated. Nitrous chilled to reduce pressure.
	Nitrous oxide spontaneously decomposes due to supercritical state or imprities in tank	5	2	4	40	Nitrous oxide is chilled to keep it below critical temperature. All personnel evacuated before fill. Tank kept sealed while in transport.
Ignition failure upon command; ignite later with personnel nearby for inspection	Wire heating time longer than expected; loose wires	4	3	4	48	Redundant ignition system minimizes chance of ignition failure. System purged off all oxidizer and disconnected from controls before personnel approach.

D. In-Flight & Recovery

Hazard	Failure Cause	S	L	D	R	Control Method
Combustion Chamber ruptures causing part of rocket to separate or tumble	Exhaust gases contacting aluminun, burning through wall	5	3	4	60	All components in combustion chamber sealed and fitted properly to ensure protection of outer wall
	Combustion instability causes pressure spike and overpressurization	5	2	4	40	Combustion chamber designed to 4.4 safety factor. Preheating region of chamber prevents instability

Rocket deviates from normal flight path and impacts ground personnel at high speed	Fins damaged before or during flight	5	2	3	30	Fins have undergone force analysis and constructed to resist flutter and deformation.
	Ignition failure causes low off the rail speed and improper stabilization	5	3	4	60	Double redundant ignitors improve reliability of ignition. Closely packed charges allow chain reaction ignition of ignitors
	Misaligned motor or mass components	5	3	4	60	Centering rings precision fit by hand and secured into rocket with high-grade adhesives. Mass components held in place by bulkeads and internal bay structures
	Nosecone crumples due to in-fligt aerodynamic foces	5	2	4	40	Nosecone has undergone stress analysis and is reinforced with fiberglass to ensure rigidity and impact strength
Recovery system fails to deploy; rocket impacts ground personnel at high speed	CO_2 charges or ganisters defective and do not deploy	5	3	3	45	CO_2 cannisters are reliable commercially produced units. Cannisters tested beforehand and thoroughly cleaned
	Batteris do not supply enough current to ignite e-matches	5	2	3	30	New batteries used and checked via multimeter for charge before installation
	Wiring improperly connected or disconnects due to in-flight forces	5	3	3	45	Ensure flight quality wiring before launch. Follow predetermined checklist upon installment.
	Altimeter malfunctions	5	2	4	40	Redundant altimeters used. Commercial altimeters used for recovery deployment.
	Shear Pins do not break upon deplment charges	5	2	3	30	Extensive ground testing done to ensure proper shearing occurs
	Parachute tangled or damaged upon ejection	5	3	3	45	Deployment bag used to protet parachute. Recovery team practices and uses care in folding parachute properly.
Main parachute deploys near apogee; rocket drifts to highway or populated area	Incorrect wiring or altimeter malfunction	4	3	3	36	Wires clearly marked to ensure proper installation; commercial altimeters used
Shock cord rips through rocket body, causing separation and falling debris	High horizontal velocity, tangling of shock cord on rocket	5	3	4	60	Only launch in proper low-wind conditions. Shock cords and parachutes folded and packed with care
Pieces of rocket come detatched and freefall due to shock forces of deployment	Improperly secured rocket parts	5	2	4	40	All mechanical connections have undergone stress calculations; fasteners checked for proper and professional installation

	Greater than expected deployment speed;horizontal velocity or drogue failure	5	3	4	60	Measures (above) taken to eliminate horizontal velocity and ensur properly timed deployment
Motor still hot upon recovery	Metal nozzle and combustion chamber retain heat; fuel gain may continue to slowly burn	4	3	3	36	Only members wearing proper PPE will be allowed to handle rocket during recovery

Appendix IV: Assembly, Preflight, and Launch Checklists

A. Airframe

Payload Integration:

1. Make sure foam padding around payload is secure.
2. Place payload into top of rocket.
3. Fit removable bulkhead onto top of payload, making sure the threaded rods go through the proper holes.
4. Screw in nuts on top of threaded rod.
5. Fit nose cone over payload.
6. Secure bolts connecting nose cone shoulder to section 1 of the rocket.

Motor integration:

1. Slide motor (with top threaded rods inserted, without nozzle attached) through section 4 of the rocket.
2. Attach nozzle by sliding the motor out slightly at the bottom of the rocket.
3. Slide motor up into section 3 of the rocket. Rotate as needed to fit bolts through the centering rings.
4. Fit threaded rods through designated holes in the thrust bulkhead.
5. Secure threaded rods with nuts.
6. Place removable bulkhead above thrust bulkhead, leaving space for plumbing.
7. Secure top of threaded rod with nuts.
8. Fill in gaps between the aeroshell and bulkhead with vacuum tape to allow for pressurization.
9. Secure bolts through the separation between sections 3 and 4.

B. Recovery

To pack the parachutes, make sure that the parachute is linked to the shock cord at the predetermined distance. A good field check of this is to hold the shock cord from where the parachute is positioned and make sure the body tubes don't make contact. Make sure that the carabenear is attached to the shock cord using a bolon knot and that it is taught. After this is checked, fold the parachute in half over itself. Next, fold the shock cords in an accordion manner, to minimize the possibility for tangling during ejection. Ensure that the ejection tubes are loaded with the black powder charges and CO2 cartridges.

Preflight Checklist

Take a thin screwdriver and locate the two pressure holes in the avionics bay that are marked with color. This indicates that the arming switches are directly adjacent to the holes. Stick the screwdriver into each hole respectively until a click is felt as the switch flips into the "on" position. A sequence of beeping should be heard from the altimeters. Confirm via the beeps and instruction manual that the altimeter is set to the correct main and drogue deployment altitudes. Following the sequence, confirm that each altimeter is giving a set of rapid beeps. This indicates that the recovery system is armed and ready for launch.

To disarm the system, take the screw-driver and flip the switches into the "off" position via the pressure holes. To confirm that the recovery system has been disarmed, ensure that the beeping has stopped.

C. Propulsion

[FLIGHT] Prometheus Check, Fill, & Fire Procedures

CONTENTS

I. Valve Check:

1. Check
    a. Regulator closed
    b. Nitrogen Bottle closed
    c. Nitrous bottle closed
2. Cycle each solenoid

a. Listen and feel for activation

II. Leak Check

1. Check
    a. Regulator closed
    b. Nitrogen bottle closed
    c. Nitrous bottle closed
    d. Dump closed
    e. Vent closed
    f. Nitrogen solenoid closed
    g. Nitrous solenoid closed
2. Open Nitrogen bottle
3. Open regulator to 30 psi
4. Open Nitrogen solenoid
    b. Listen and feel for leaks in ground plumbing, on tank, inside CC
5. Close Nitrogen Solenoid
6. Open Dump Solenoid
7. Increase nitrogen regulator pressure to 150 psi
8. Clear personnel from vicinity of motor and inform personnel we will be performing a 150 psi leak check
9. Open nitrogen solenoid
10. When PT reading stabilizes, close nitrogen solenoid
11. Watch tank pressure for 45 sec to check for any decrease
12. Open Dump (pad cleared, safe to approach)

III. Fill & Fire

1. Check
    a. Launch Pad cleared besides 2 final personnel
    b. Regulator closed
    c. Nitrogen Bottle closed
    d. Nitrous bottle closed
    e. Dump open
    f. Vent closed
    g. Nitrogen solenoid closed

h. Nitrous solenoid closed
2. Open Nitrogen bottle valve
3. Check and record Nitrogen Pressure
4. Open regulator to 200 psi
5. Open Nitrous Bottle Valve
6. Check and Record Nitrous Pressure
7. Connect Ignition Leads
8. Evacuate launch pad area
9. Close Dump
10. Inform pyro-op that we will begin our fill now
11. Open Nitrous solenoid
12. When pressure reaches 50 psi below Nitrous bottle pressure, open vent until pressure is 75 psi below bottle pressure
    a. Repeat until 10.75 lbs of nitrous filled OR thick white plume exits vent indicating a full fill
13. Close Nitrous solenoid, inform pyro-op that tank is full and are waiting for pressure to build
14. Proceed when pressure reaches 825 psi or stabilizes
15. Begin ignition sequence countdown from 10
16. T-3 sec: Arm ignition safety switch
17. T-1 sec: Activate ignition, leave in ON position

IV. If ignition successful:

1. Deactivate ignition switch upon confirmed ignition of grain
2. Wait until burn complete + 10 sec
3. Open Nitrogen solenoid
    a. Wait 5 sec
4. Close Nitrogen solenoid
5. Approach launch pad
6. Close Nitrous bottle
7. Open Nitrous solenoid
8. Open Nitrogen solenoid
9. Close Nitrogen bottle
    a. Wait 3 sec
10. Close Nitrogen solenoid
11. Close Nitrous solenoid

All Clear

V. If ignition NOT successful at T+5 sec:

1. Cycle Ignition 1 sec on, 1 sec off for 3 cycles
    a. If Ignition Successful refer to ignition success procedures
    b. If unsuccessful, continue below
2. Deactivate ignition
3. Inform pyro-op that we will be dumping oxidizer
4. Open Dump
    a. Wait until PT confirmation of atmospheric pressure + 5 sec
5. Close Dump
6. Open Vent
7. Open Nitrogen Solenoid
    a. Wait 10 sec
3. Close Nitrogen solenoid
4. Close Vent
5. Open Dump
6. Approach launch pad
7. Proceed to Launch Pad System Flush (**VIII**)

VI. Vent failure

1. Close Nitrous Solenoid

2. Cycle Vent in 1 sec cycles x5
    a. Proceed with normal fill if vent actuates, otherwise continue with step 3
3. Announce that fire is aborted and we will proceed to Dump oxidizer
4. Open Dump
    a. Wait until tank pressure reads atmospheric + 10 sec
5. Close Dump
6. Open Nitrogen Solenoid
    a. Wait 10 sec
7. Close Nitrogen solenoid
8. Open Dump
9. Approach launch pad
10. Detach ignition
11. Proceed to Launch Pad System Flush (**VIII**)

VII. Pressure Transducer Failure

1. Close Nitrous
2. Open Vent
    a. If pressure transducer regains function, proceed with normal fill procedures
    b. If pressure transducer remains non-operational after 10 sec, inform pyro op that we will dump oxidizer due to instrumentation failure
3. Open dump
4. Wait until no oxidizer seen exiting dump valve or 30 sec if no visual
5. Close dump
6. Open Nitrogen
    a. Wait 10 sec
7. Open Dump
8. Close Nitrogen
9. Proceed to Launch Pad System Flush (**VIII**)

VIII. Launch Pad System Flush (in case of no ignition)

1. Close Nitrous bottle
2. Open Nitrous solenoid
    a. Wait 3 sec
3. Open Nitrogen Solenoid
    a. Wait 3 sec
4. Open Vent
5. Close Dump
    a. Wait 5 sec
6. Close Nitrogen Solenoid
7. Close Nitrous Solenoid
8. Open Dump
9. Close Nitrogen bottle
10. Open Nitrogen solenoid
    a. Wait 1 sec
11. Close Nitrogen Solenoid
12. Close Regulator

All lines are flushed with Nitrogen and depressurized, bottles closed, solenoids in natural position

Appendix V: Engineering Drawings

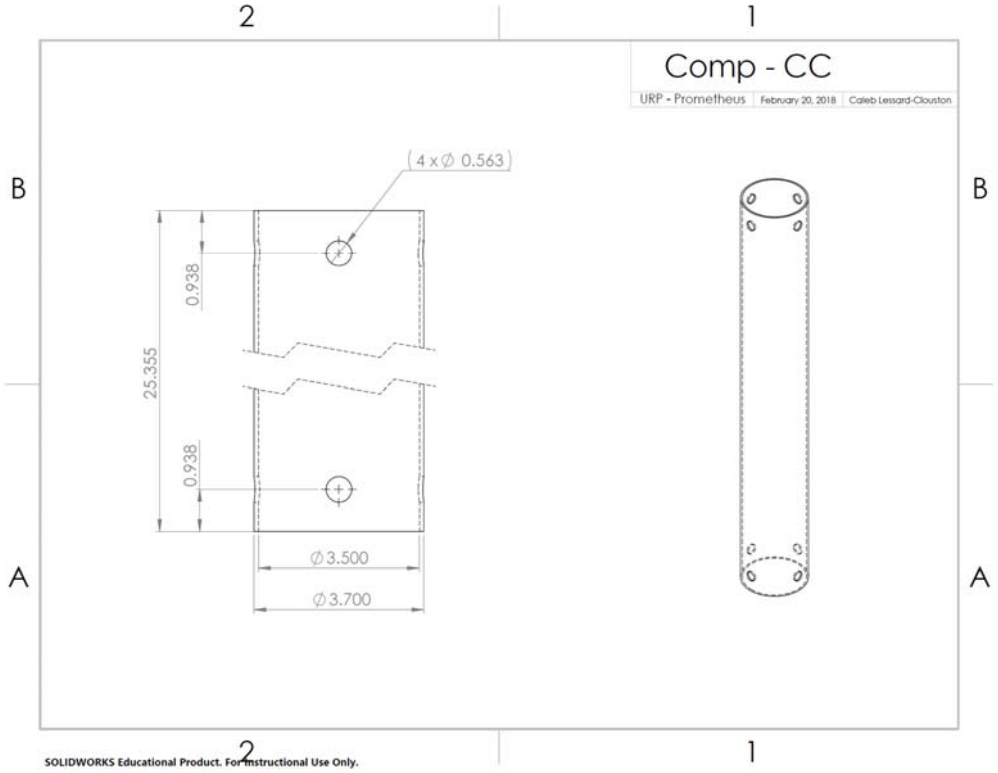

Figure A6.0.1 Combustion chamber engineering drawing

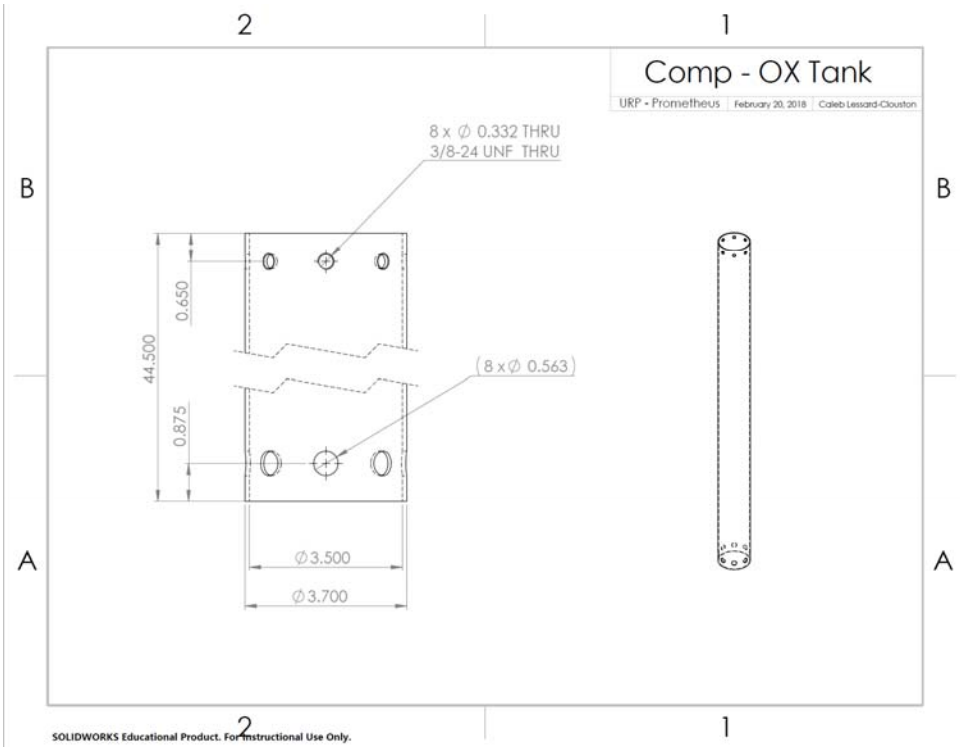

Figure A6.0.2 Oxidizer tank engineering drawing

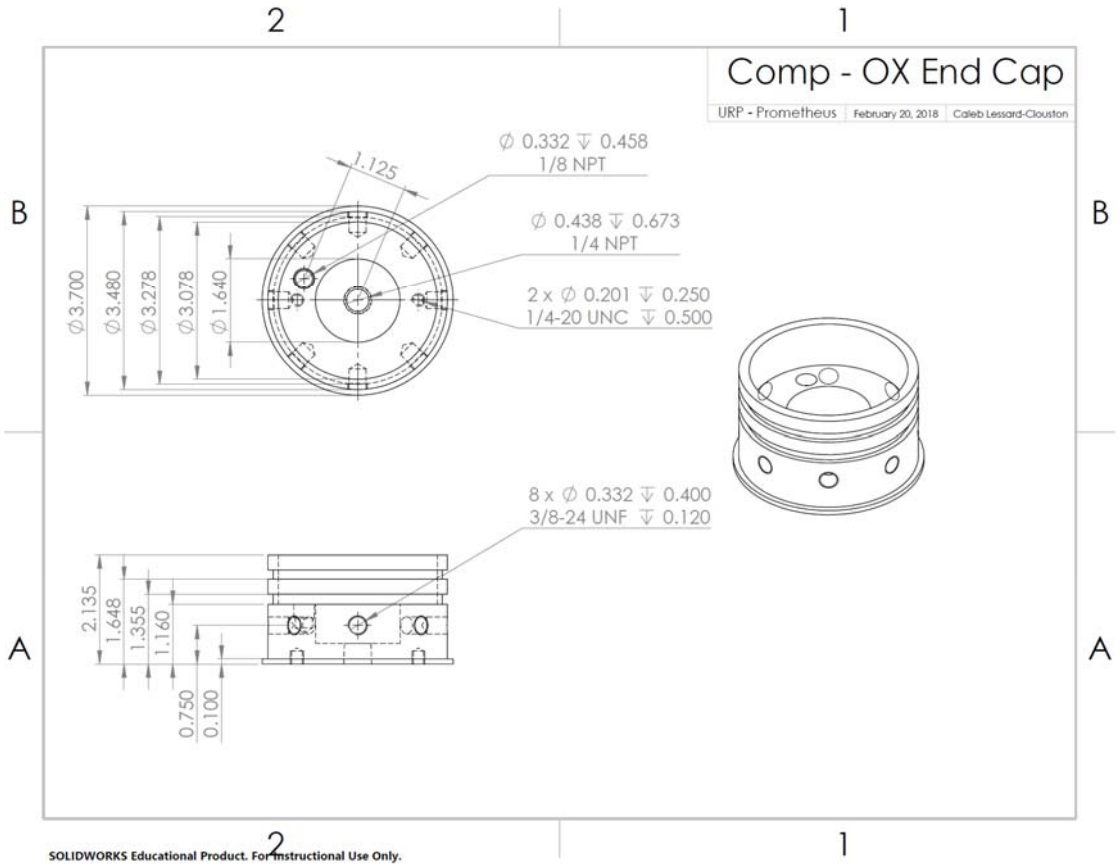

Figure A6.3 Oxidizer tank end cap engineering drawing

Acknowledgements

Project Prometheus would like to thank our postdoctoral advisor, Dr. Daniel Pineda for his invaluable guidance and encouragement. Dr. Pineda goes above and beyond his job description every day for us and it does not go unnoticed. From his wisdom at early morning FAR trips to his persistence at late nights in the machine shop, none of this would be possible without him.

The Prometheus team would like to thank UCLA Engineering and especially the Department of Mechanical and Aerospace Engineering for the support and resources necessary for our success. We would also like to thank Dr. Spearrin and Dr. Wirz, our faculty advisors, as well as Dr. Lynch, current chair of the MAE Department for supporting us directly and being our faculty voices.

Prometheus finally would like to thank all the older members of Rocket Project at UCLA who believed in our big aspirations, gave us the guidance and support necessary for success, and taught us everything we know.